Int. J. Heat Mass Transfer. Vol. 20, pp. 899–910. Pergamon Press 1977. Printed in Great Britain

TEMPERATURE AND CONCENTRATION PROFILES IN TRANSIENT GAS FLOWS BY ROTATIONAL RAMAN SCATTERING

J. R. SMITH* and W. H. GIEDT†

(*Received* 29 *September* 1975 *and in revised form* 6 *September* 1976)

Abstract—A new technique is presented for simultaneously measuring temperature and concentration profiles in diatomic gases during transient flows. Using a continuous argon laser, rotational Raman scattered light from the sample gases is dispersed by a single-pass spectrometer; the resulting spectra are detected by an image intensifier and a low-light-level television camera every 0.033 s.

A system based on this technique was developed and temperature and concentration distributions determined in a right circular cylinder during axial injection of deuterium at 200 atm and 430 K into deuterium at 100 atm and 300 K. Temperature and concentration profiles are presented at selected times during the injection process.

NOMENCLATURE

B_e, equilibrium molecular rotational constant [cm^{-1}];
B_0, molecular rotational constant (molecule in the vibrational ground state), $= B_e - 1/2\alpha_e$ [cm^{-1}];
c, speed of light;
C, system sensitivity constant;
D, vibrational influence coefficient, $= 4B_e^3/\omega_e^2$, and inlet tube inside diameter;
E_J, energy of the Jth rotational energy level [ergs];
h, Planck's constant;
I, light intensity;
J, rotational quantum number;
k, Boltzmann's constant;
L, length of laser beam imaged onto detector [cm];
N, number density of gas molecules [cm^{-3}];
Q_r, rotational partition function;
R^n, nuclear spin influence coefficient, $= s/(s+1)$;
s, nuclear spin;
S, separation distance between gas inlet and laser beam [mm];
S_J, rotational line strength (transition probability);
T, absolute temperature [K];
y, position along the laser beam, measured from the axis of the test cell [mm].

Greek symbols

α_e, molecular anharmonicity constant [cm^{-1}];
γ, rotational–vibrational interaction coefficient, $= 2B_e/\omega_e$;
θ, characteristic rotational temperature, $= hcB_0/k$ [K];
ν_0, laser frequency [cm^{-1}];
ν_J, frequency of the Jth rotational Raman transition [cm^{-1}];
σ, rotational Raman cross section [cm^2/s];
χ, experimentally determined constant used in the calculation of the line-strength correction factor, f_J;
Ω, solid angle subtended by the collection lens [sr];
ω_e, molecular vibration constant [cm^{-1}].

INTRODUCTION

MEASUREMENTS of static temperature distributions in flow fields are frequently required in heat-transfer research and design. In many cases it is undesirable or impossible to use a conventional probe, such as a thermocouple. Therefore, remote-sensing optical techniques have received considerable attention in recent years. Examples include the use of interferometry, schlieren techniques, and i.r. absorption in known density fields to infer static temperatures. Although these are remote methods, they suffer the major defect of integrating over a path (or field of view) and hence are limited to two-dimensional flow fields.

The availability of lasers has added the possibility of utilizing the Raman scattering effect for temperature and species concentration measurements [1]. When a laser beam is focused into a small volume of particulate-free gas,* the gas (stationary or flowing) will not be perturbed if the incident-radiation power densities are low enough to preclude stimulated Raman scattering [3] or ionization [4] and the individual photon energy is less than the dissociation energy. The quantum mechanical explanation of the Raman effect is that

*Member of Technical Staff, Combustion Research Division 8351, Sandria Laboratories, Livermore, CA 94550, U.S.A.

†Associate Dean, College of Engineering, University of California, Davis.

*The interaction of the laser beam with particulates and its effects on Raman measurements are discussed in [2].

when a photon of frequency ν_0 and energy $h\nu_0$ interacts with a molecule, it can be scattered either elastically (Rayleigh scattering) or inelastically (Raman scattering). In inelastic scattering, the photon either gives up part of its energy to the scattering system or takes energy from it. The photon can exchange only amounts of energy that are equal to the energy differences between the stationary states of the system. The requirements for efficiently producing and collecting Raman scattered light from small gas volumes have been established by Barrett and Adams [5]. Since the intensity of the Raman scattered light is low, relatively long observation periods are normally needed. This time may be shortened by collecting light at many wavelengths simultaneously by using an image intensifier and television camera as demonstrated by Bridoux and Delhaye [6]. An alternate technique developed by Widhopf and Lederman [7] to make fast measurements of species concentrations incorporated a pulsed ruby laser and a photomultiplier tube.

Over a moderate temperature range centered around room temperature, practically all of the molecules of diatomic gases are in the lowest, or ground vibrational, energy level. They are, however, distributed throughout many of the available rotational energy levels. This distribution is dependent on the temperature. For example, the remote determination of temperatures in nitrogen from rotational Raman spectra was investigated by Salzman, Masica and Coney [8]. The results of these investigators suggested that it should be possible to incorporate a high-powered or pulsed laser, an image intensifier, and a low-light-level television camera into a Raman scattering system which would be capable of measuring local static temperatures in both steady and transient gas flows. The objective of the study described herein has been to develop such a system with the additional capability of measuring the temperature distribution over a few centimeters. A cylindrical gas cell with provision for axial gas injection was selected to demonstrate the capabilities and to investigate the limitations of the rotational Raman temperature and concentration profile measurement system.

ROTATIONAL RAMAN SCATTERING THEORY

The Raman effect is an electromagnetic-radiation-scattering phenomenon in which the scattered radiation is shifted in frequency from the incident radiation frequency, the shift in frequency being governed by the nature of the scattering species. Though such scattering may be produced in solids, liquids or gases, the present discussion will be limited to diatomic gases since they yield particularly simple rotational spectra and constitute a fluid medium of widespread practical importance.

Rigid rotator

The stationary states or permitted rotational energy levels of a diatomic molecule idealized as a rigid rotator are found by solving the Schrodinger equation [9]. These levels are given by (see Nomenclature for definition of terms)

$$E_J = hcB_0J(J+1) \tag{1}$$

in which J can have values of 0, 1, 2 . . .

The selection rule for the rigid rotator is $\Delta J = \pm 1$ [10], which gives the allowed transitions between energy levels. Conventionally, $\Delta J = J' - J''$, where J' always refers to the upper state and J'' the lower state. Hence, ΔJ can only be positive.

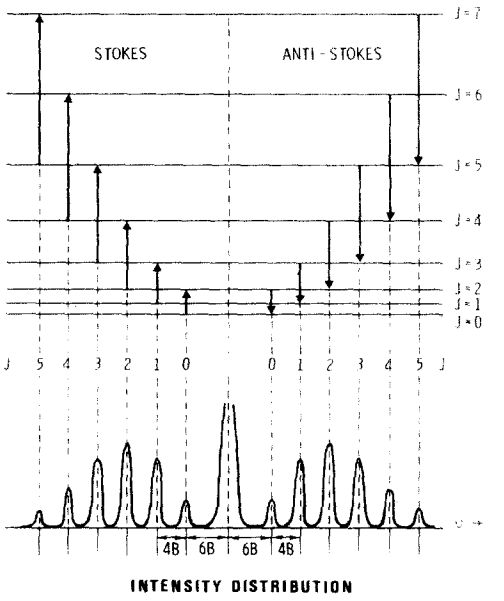

FIG. 1. Rotational energy level diagram and Raman spectrum intensity distribution for a diatomic molecule.

This behavior is illustrated in Fig. 1 in terms of a series of discrete energy levels whose energy increases quadratically with increasing J, a condition which gives rise to a spectrum of equally displaced lines. Because of the selection rule, the frequency shift is given by

$$|\Delta\nu| = B_0(J+2)(J+1+2) - B_0J(J+1) = 4B_0(J+\tfrac{3}{2}) \tag{2}$$

in which J denotes the lower state and the primes have been deleted for convenience. The spectral lines associated with the transitions that decrease the energy of the incident photon and hence increase the energy of the molecule are called Stokes lines. Spectral lines due to increases in incident photon energy are known as anti-Stokes lines.

The intensities of the individual rotational Raman lines are given by [10]

$$I_J = CN_J(\nu_0 \pm \Delta\nu)^4S_J \tag{3}$$

where I_J is the intensity of the Jth rotational line; C is a system-dependent constant accounting for incident light intensity, Raman cross section for interaction, scattered-light collection efficiency, etc.; N_J is the number of molecules in the initial energy level. Note that $\Delta\nu$ is negative for Stokes transitions and positive for anti-Stokes transitions. The number of molecules in the initial energy state is given by the thermal

distribution [11] among the rotational levels

$$N_J = \frac{NR^n}{Q_r}(2J+1)\exp(-E_J/kT). \quad (4)$$

Here Q_r is the rotational partition function, given by

$$Q_r = \sum_{J=0}^{\infty} R^n(2J+1)\exp[-J(J+1)hcB_0/kT]. \quad (5)$$

The line strength used in equation (3) was determined by Placzek and Teller [12] as

$$S_J = \frac{3(J+1)(J+2)}{2(2J+3)}. \quad (6)$$

In homonuclear molecules (e.g. H_2, D_2, N_2, etc.) the exchange of nuclei with nuclear spin s occurs but does not necessarily lead to a completely identical state since the nuclei may still differ by the orientation of their spins. The spin vectors form a resultant that is the total nuclear spin of the molecule. The ratio of the statistical weights of the antisymmetric and symmetric rotational levels is given by the nuclear influence coefficient R^n where $n = 1$ for para modification and $n = 0$ for ortho modification. Note that, for heteronuclear molecules, n must be taken as zero.

Nonrigid rotator

For molecules with large rotational constants (such as deuterium), or at high temperatures, the stretching of the molecule due to centrifugal force changes the rotational speed and must be taken into account. Equation (1) then becomes ([10], p. 103)

$$E_J = hcB_0\left\{J(J+1) - \frac{D}{B_0}[J(J+1)]^2\right\}. \quad (7)$$

The frequency shift given in equation (2) is modified to

$$|\Delta\nu| = (4B_0 - 6D)(J+\tfrac{3}{2}) - 8D(J+\tfrac{3}{2})^3. \quad (8)$$

Not only must energy-level changes be accounted for but, as James and Klemperer [13] have pointed out, the transition probability of a rigid rotator must be modified by a correction term

$$f_J = 1 + \frac{2\gamma^2}{\chi}(J^2+3J+3). \quad (9)$$

This term must be used as a multiplier of the line strength, S_J, given by equation (6). The χ term in equation (9) is an experimentally determined constant that may be derived from line intensity ratios in the Raman rotational–vibrational spectrum. Details of this measurement and calculation for D_2 are given in [14]. The χ value for D_2 was found to be 0.44 ± 0.08.

Including the above modifications yields the following expressions for the Stokes intensity:

$$I_{\text{Stokes}} = \frac{CR^nNf_J(J+1)(J+2)(\nu_0-\Delta\nu)^4}{Q_r(2J+3)} \times \left\{\exp\left(-\left\{J(J+1)\left[1-\frac{D}{B_0}J(J+1)\right]\right\}\theta/T\right)\right\}. \quad (10)$$

Substituting $J+2$ for J in the exponential term yields a similar expression for anti-Stokes intensities.

The gas temperature and concentration can be determined from experimental intensity values. For this purpose the partition function Q_r was approximated by a relation of the form Ae^{-HT} (with $A = 17.658$ and $H = 352.8$ the maximum error is about 1% for deuterium over the temperature range of 300–500 K). The result can be written in the form

$$\ln\left\{\frac{I_s(2J+3)}{R^nf_J(J+1)(J+2)(\nu_0-\Delta\nu)^4}\right\} = -\left\{J(J+1)\left[1-\frac{D}{B_0}J(J+1)\right] - H/\theta\right\}\theta/T - \ln\left(\frac{A}{CN}\right). \quad (11)$$

Plotting the left side vs the first term on the R.H.S. of equation (11) on semi-logarithmic coordinates yields a straight line of slope $-\theta/T$. A least-squares routine was used to determine the best slope through the data. This technique uses all of the available data from the Stokes wing of the pure rotational Raman spectrum. Researchers in the past [15, 16] have taken the ratio of two regions of the Raman spectrum. Data from the anti-Stokes wing could similarly be used.

The last term in equation (11) contains the number density N and is the ordinate intercept of the straight-line fit to the data. The number density is thus given by

$$N = \left(\frac{A}{C}\right)e^b \quad (12)$$

where b is the intercept. Recall that the constant A is from the relation used for the partition function; the constant C is a system constant determined by the experimental arrangement. Therefore, if measurements are made at a known density of a pure species, the value of C may be determined.

Spectral line shape

The shape of the individual rotational Raman lines is the result of the interaction between the Doppler-broadened incident photons and the natural line and pressure-broadened molecular energy levels. This actual line shape is further changed by the imperfections of the analyzing and recording equipment [17].

A fused-quartz etalon was used within the laser cavity, thus yielding a laser line width of only $0.0024\,\text{cm}^{-1}$ within the 514.5 nm laser gain profile. It should be emphasized that the laser line width was reduced to permit the use of an iodine absorption filter and not to improve the laser spectral purity for resolution purposes.

Natural-line broadening results from the uncertainty associated with the values for the initial and final energy levels. Murray and Javan [18] found the natural line width of deuterium to be $0.053\,\text{cm}^{-1}$. The natural-line shape is Lorentzian. The pressure-broadened line width in these experiments was of the order of $0.35\,\text{cm}^{-1}$ and is essentially Lorentzian.

The total Raman-scattering line width (of an individual line) is the integral of the product of the

distributions for the Doppler-broadened, natural-line broadened and pressure-broadened contributions over all frequencies. Such an integration must be carried out numerically. However, the sum of the individual contributions may be used to estimate the total line width. (This simple technique always yields estimates that are slightly larger than the integral method. Therefore, the total Raman line width is taken to be about 0.40 cm^{-1}.)

The spectrometer entrance slit width was 200 μ, a value which corresponds to about 7 cm^{-1} for the dispersion used. Thus the spectrometer distortion is the dominant factor in determining the Raman line shape in this study. An evaluation of the transmission characteristics of the spectrometer suggested the use of a Gaussian slit function. The spectral intensities as a function of wave number for the Stokes wing of D_2 were computed for three different temperatures as shown in Fig. 2.

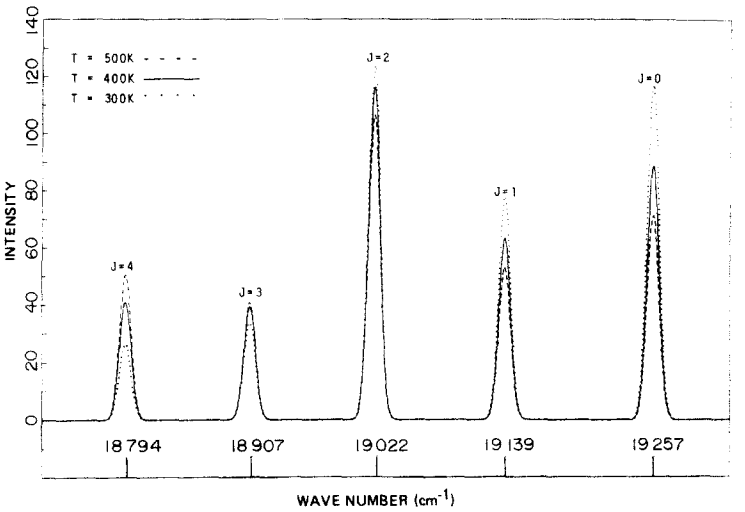

FIG. 2. Rotational Raman spectrum of Stokes wing for D_2.

EXPERIMENTAL EQUIPMENT AND TECHNIQUE

The components and the optical path of the system developed are illustrated schematically in Fig. 3. A high-power continuous wave argon laser* was used to produce 3.5 W of monochromatic light at a wavelength of 514.5 nm.† The laser beam was focused at the center of the test cell by a lens of 100 mm focal length. The TEM_{00} (transverse mode with Gaussian intensity distribution) laser beam, together with the diffraction-limited focusing capability of the lens, makes it possible to describe precisely the shape of the laser beam within the test cell [5]. It is important that this arrangement be used because it controls the location and spatial resolution of the laser beam. The configuration described yields a long, nearly cylindrical beam of light of approximately 50-μ dia. Within this cylinder of light, all the Raman scattering takes place.

Perpendicular to the focused laser beam and on axis with the test cell, a camera lens with an 85 mm focal length and an $f/1.8$ aperature collects the scattered light. The collection lens focuses an image of the scattering volume (defined by the focused laser beam) onto the entrance slit, and within the $f/6.3$ acceptance cone, of a spectrometer. The spectrometer used was a Jarrell-Ash® 3/4-m, single-pass instrument which utilized a Bausch and Lomb® 1800-groove/mm grating specially selected for low-ghost characteristics. The plane of polarization of the incident laser beam coincided with the axis of the collection optics in such a way as to decrease the Rayleigh-scattered light [5].

In order to further reduce the magnitude of the Rayleigh-scattered light entering the spectrometer, an iodine filter cell (which has a sharp absorption transition within the 514.5 nm laser gain profile) was placed between the collection lens and the spectrometer entrance slit. An iodine filter in conjunction with an etalon-tuned argon laser can absorb several orders of magnitude of the Rayleigh-scattered light without significantly decreasing the rotational Raman scattering [19]. The tilt of the etalon tunes the laser to operate in a single longitudinal mode at the iodine absorption frequency. This technique was used at the expense of nearly 50% of the laser output power but resulted in significant improvements in the signal-to-noise ratio.

The spectrum from the spectrometer was focused by another lens of 85-mm focal length onto a 3-stage image-intensifier tube.* This 40-mm diameter tube has a spatial resolution of about 25 line pairs per mm and a maximum radiant power gain of 100 000. The image intensifier was typically used at a gain of 20–30 000 where it yielded better signal-to-noise ratios. The

*Spectra-Physics® model 170-03.

†Initial use of a pulsed-ruby laser which would have made possible a time resolution of about 1 ms, was unsuccessful due to test chamber window fluorescence at 694.3 nm from residual chromium in the sapphire window. This fluorescence thus added to the apparent Rayleigh line intensity making rotation Raman spectra detection very difficult using a ruby laser.

*RCA® 8606 image intensifier.

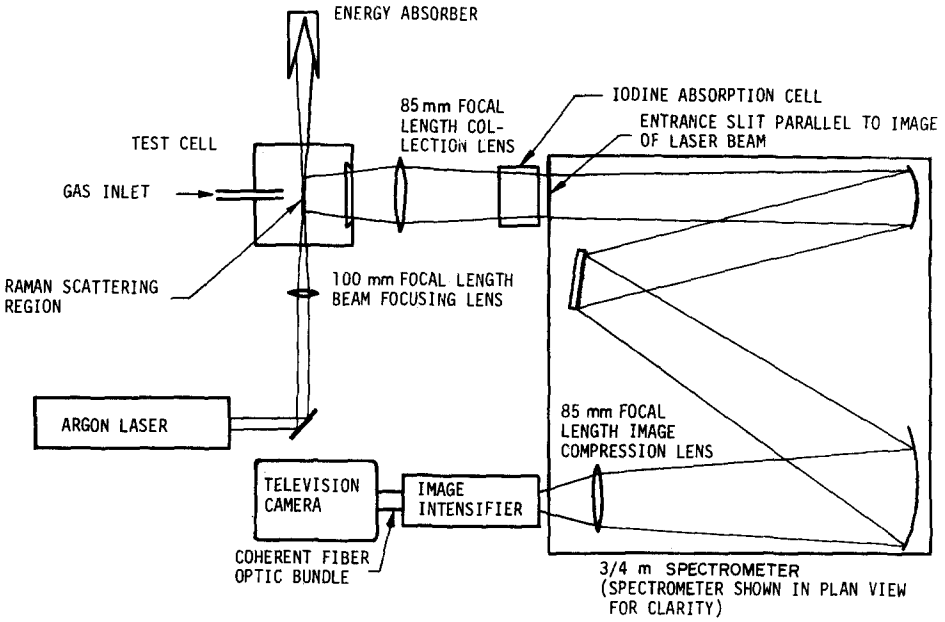

FIG. 3. Schematic of optics for rotational Raman profile system.

intensifier was coupled to a low-light-level television camera* by a coherent fiber-optic bundle 25 mm long. This bundle length is necessary to prevent arcing between the television camera and image intensifier which are at large electrical potential differences. Only the central 25 mm of the image intensifier was used to avoid excessive pincushion distortion. The low-light-level television camera was modified to use a SIT tube (silicon intensified camera tube) for additional sensitivity. The television camera used the standard commercial format, i.e. 2:1 interlace of 525 horizontal scan lines at 30 frames per second. This means that the odd lines of the 525 total lines are scanned for the first field, then even lines for the second field. The time required to scan each field is 16.7 ms, but the time between the scanning of any given line is twice this amount or 33.3 ms. Therefore, such a system, when used with a continuous laser, has at best a time resolution of 33.3 ms.

No exit slit is used on the spectrometer. This allows the entire rotational Raman spectrum to be seen simultaneously without moving the spectrometer grating. A view of the television monitor as shown in Fig. 4 has as coordinates, wavelength in the horizontal direction and position along the laser beam in the vertical direction. Each television scan line represents a separate rotational Raman spectrum corresponding to a specific location within the test cell. With the aid of the theoretical relationships between intensity and temperature, and intensity and concentration developed in the previous sections, a single frame of television data yields temperature and concentration profiles along the path of the laser beam.

The test cell used in this experiment was a right circular cylinder with a maximum working pressure of 340 atm. The most notable feature of the cell is its conical sapphire collection window which is so shaped as to maintain the entire window in compression at the working pressure. The I.D. and length of the test cell is 25.4 mm. The face of the end plug is threaded to accept various tubes that are used to change the distance between the inlet and the laser beam. All the tubes used in this experiment had 2.0 mm inside diameter and 5.0 mm O.D.

The high pressure plumbing arrangement used a source vessel (accumulator) with a volume of 120 cm^3, while the test cell had a volume of 12.9 cm^3. All of the tests were run with 100 atm initial pressure in the test cell and 200 atm in the accumulator. Thus the source pressure decreased less than 10% during the filling process. The method used for injecting warm gas was by electrically heating the last 100 mm length of tubing immediately adjacent to the test cell. The injected gas temperature was 430–440 K during most of the fill process, but tended to rise to nearly 450 K as pressure equilibrium was approached. A multiple-holed orifice was placed between the accumulator and the heated section of the transfer tubing to slow the gas flow. The resulting transient gas filling characteristics versus filling time are shown in Fig. 5. No special precautions were taken to remove particulates from the gas.

Test procedure

After 10 min of heating to ensure uniform tube temperature, an air-operated valve was opened (actuation time 20–40 ms), allowing the test cell and the accumulator to come to pressure equilibrium. A light-emitting diode located within the spectrometer was illuminated for 10 ms when valve actuation was started. This provided a video signal at start time. The valve

*Westinghouse® model 606.

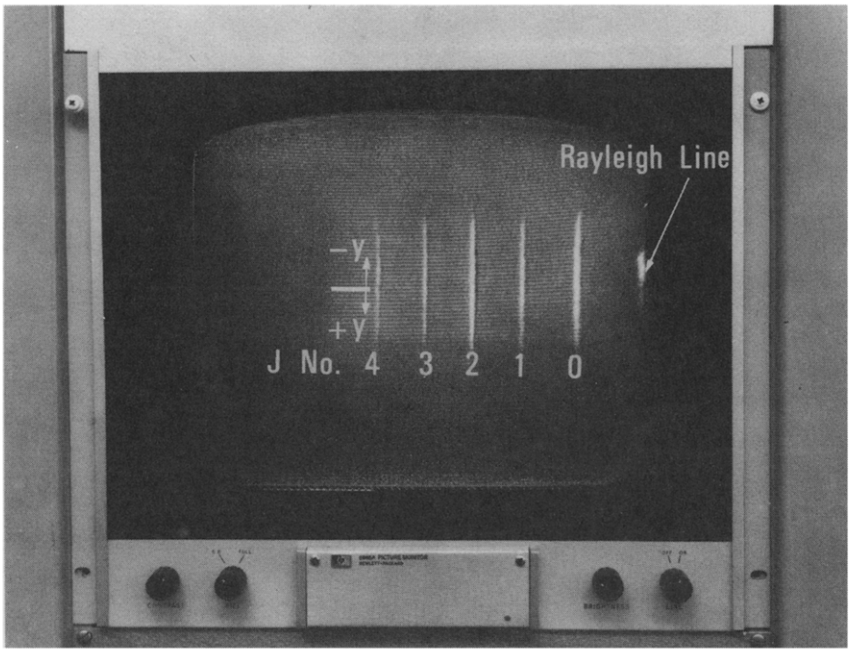

FIG. 4. Television monitor view of Stokes rotational Raman spectrum of D_2 (top of test cell at bottom of screen due to inverting optics of the image intensifier).

remained open for 10 s. As shown in Fig. 5, the fill time for the test cell was about 2 s. During this time, the rotational Raman spectra were recorded on a 1 2-in video tape recorder.* Prior to each transient fill, the temperature is measured by a calibrated thermocouple, and the gas pressure by a calibrated pressure gauge in the test cell. These video frames of the D_2 spectra at known temperature and density are used as the calibration spectra to account for variation in system sensitivity as a function of wavelength and time.

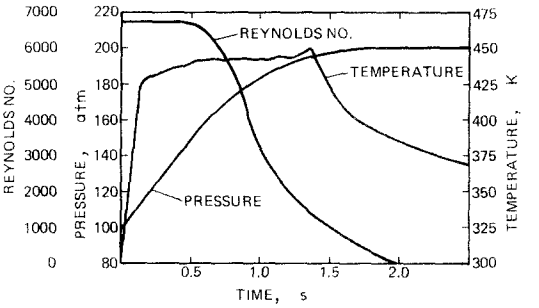

FIG. 5. Test cell pressure, Reynolds number and inlet temperature vs time.

Scattering signal estimate

An estimate of the fraction of incident light that is scattered in the Raman spectrum may be made by using the relation [7]

$$\frac{I_{\text{scattered}}}{I_{\text{incident}}} = \left(\frac{\nu_j}{\nu_0}\right)^4 \frac{NL\sigma\Omega}{4\pi}. \tag{13}$$

For rotational scattering $\nu_j \simeq \nu_0$; N is the number of molecules per cm^3, equal to 2.69×10^{19}/cm^3 ama; σ is the rotational Raman cross section for D_2, which is $\sim 2.2 \times 10^{-30}$ cm^2/s;† Ω is the solid angle subtended by the collection optics, which is 0.067 sr for the $f/1.8$, 85 mm focal length lens used; and L is the length of laser beam that is being imaged onto the detector. The total length of laser beam viewed was 1.2 cm which was imaged onto some 60 scan lines (of one television field) of the television camera. Since alternate lines were not used, $L = 1.2$ cm/120 lines = 0.01 cm. Evaluating equation (13) yields $I_s/I_i = 3 \times 10^{-15}$ ama. This is the fraction of the incident light that falls on the entrance slit of the spectrometer. Estimating the throughput of the spectrometer at 30%, the transmission of the iodine cell at 10%, and the transmission of the imaging lens between the spectrometer and the image intensifier at 85% gives the fraction of light incident on the face of the image intensifier as $I_s/I_i \simeq 8 \times 10^{-17}$ per ama.

Of the 3.5 W of incident laser power, approximately 3 W passes through the test cell. The difference is due to focusing-lens losses and window and mirror transmission losses. Note that the intensity decrease due to Raman scattering is trivial since it is of the order of 10^{-8}/cm, even at 150 ama densities. Since the television camera tube is scanned 30 times per second, the incident energy during one scan is (1/30 s)(3 W) = 0.1 J. This corresponds to 2.58×10^{17} photons at 514.5 nm. Therefore, the number of photons incident on the image intensifier is about 20 per amagat density. The quantum efficiency of the photo cathode of the image intensifier is nearly 15% at 514.5 nm giving a photoelectron production of about 3 per amagat density.

These estimates of the photoelectron production reveal why it is necessary to operate at high densities

*Sony® model 3650 video tape recorder.

†This is an estimate based on the rotational Raman cross-section for nitrogen of [20] and the polarizability of deuterium of [21].

when both very good spatial resolution and moderately good temporal resolution are desired. Even at 100 ama densities, the statistical variation of the video signal is large since it is proportional to the square root of the number of photo-electrons produced, or about $\pm 6\%$.

SYSTEM CALIBRATION AND DATA REDUCTION PROCEDURE

A very large amount of spectral data was obtained, and a comparatively lengthy calculation procedure was involved in determining local temperature and concentration. A typical test required a minimum of 50 frames of video data. Each frame has 60 lines of data that were digitized into 2048 intervals. Thus a single test involved over six million data points. All data had to be examined to determine the individual rotational Raman line intensities for use with the equations developed in the Rotational Raman Scattering Theory portion of this paper in order to compute temperature and concentration profiles during the filling process. To accomplish this task, a special digitizing system and a large digital computer were used. After each frame (including 20 pretest calibration frames) had been digitized, an effective baseline was determined, thus accounting for spatial sensitivity variation of the optical system—largely attributable to the image intensifier. This method of calibration also compensates for any non-uniform absorption of the Raman spectrum by the iodine filter. The procedure is described in detail in [14].

The dynamic spectra were time-averaged over three frames and space-averaged over every pair of adjacent scan lines. Time-averaging of three frames gives a time resolution of 0.10 s and the spatial-averaging of adjacent scan lines results in some loss in space resolution —a compromise made to achieve better photon statistics. The resulting spatial resolution is 0.2 mm along the laser beam.

EXPERIMENTAL RESULTS AND DISCUSSION

An example of a rotational Raman spectrum of deuterium as recorded by the television system is shown in Fig. 6. This is the video signal from a single scan line of the television camera. Both Stokes (left side) and anti-Stokes wings are shown. The Stokes wing was used because of its stronger signal.

An important aspect of any new measurement technique is its accuracy. In order to determine the accuracy of the temperature computed from the rotational Raman profile system, a series of measurements were made with quiescent deuterium at 150 atm pressure and room temperature prior to each test. A chromel–constantan thermocouple near the center of the test cell was used to determine the actual gas temperature. Temperatures at various locations were calculated from the spectra of each test. One standard deviation of the temperature error is 9.2 K, and the bias of the mean from the true temperature is -2.4 K.

The absolute accuracy of the density measurements is about $\pm 10\%$, based on an estimate of the combined precision of the recording and digitizing equipment. The relative density (i.e. that within a given profile) is probably much better.

Temperature and density profiles

Temperature and density profile data were taken with seven different axial injection flow configurations. The length of the inlet tube was varied to give profiles at distances ranging from 0.49 to 7.82 tube diameters from the laser beam to the tube inlet. All tests were done with the same initial conditions of deuterium at 200 atm source pressure and 100 atm test-cell pressure. Temperature and density profiles for all seven test cell configurations are presented in [14].

The experimental temperature profiles for $S/D = 0.94$, $S/D = 4.06$ and $S/D = 7.82$ are presented in Figs. 7–9. Although data were taken continuously from the time of valve opening to 5 s afterwards, only a few of the 50 profiles obtained during this time are presented. The early time (0.1–0.8 s) profiles are for a condition of essentially constant inlet Reynolds number. The first few of these profiles are at times comparable to the period over which the spectral data were averaged (0.1 s). The late-time profiles (1.5–5 s) give an indication of the decay of the jet when pressure equilibrium is

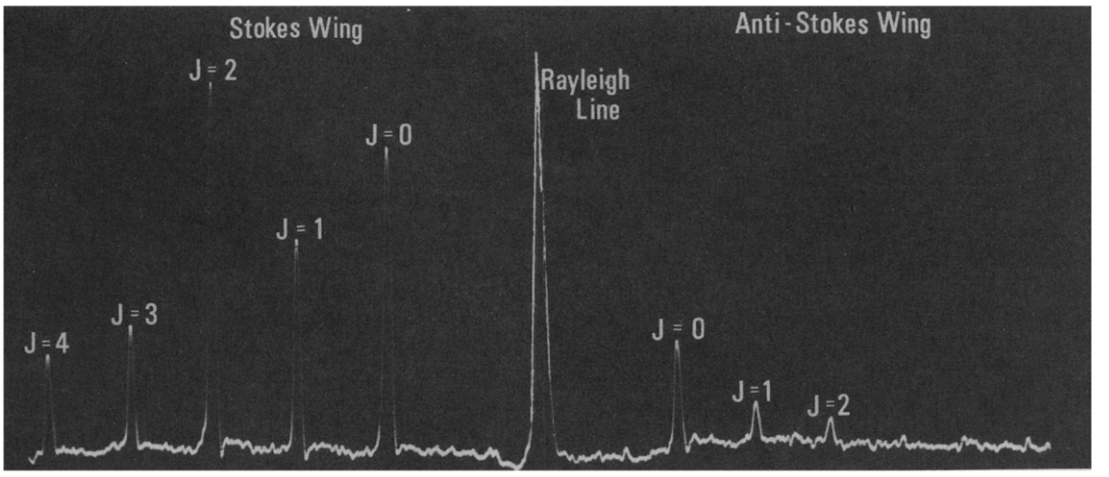

FIG. 6. Rotational Raman spectrum of D_2 at room temperature.

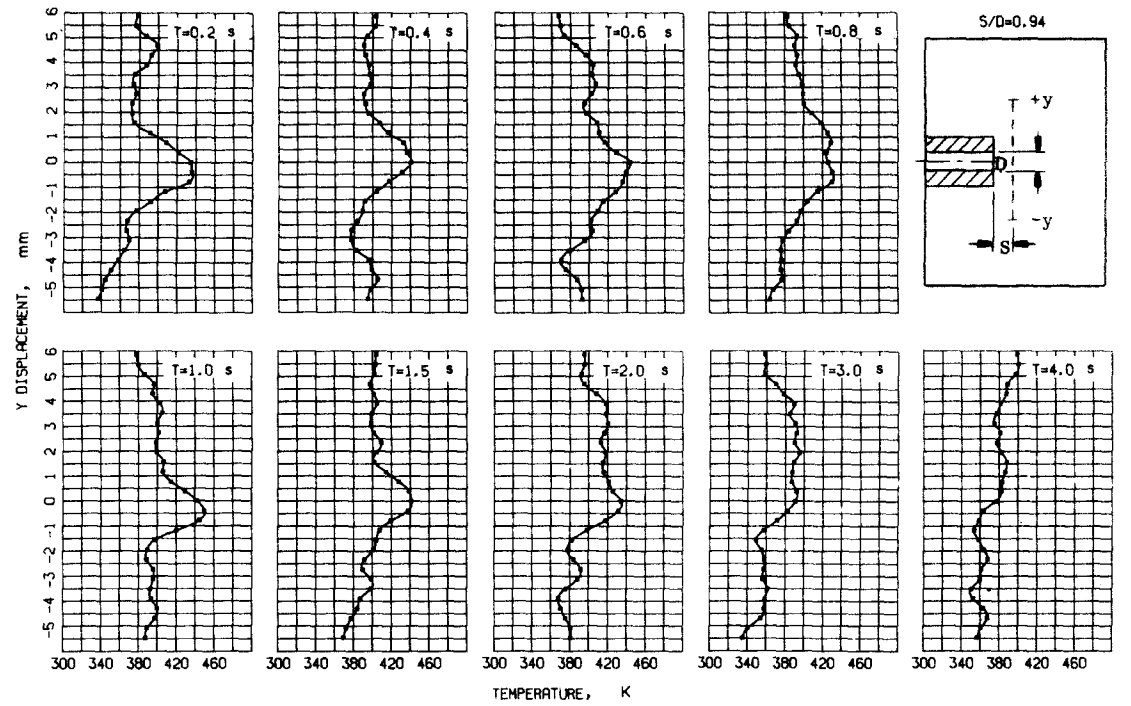

FIG. 7. Temperature profiles at 0.94 tube diameters from inlet.

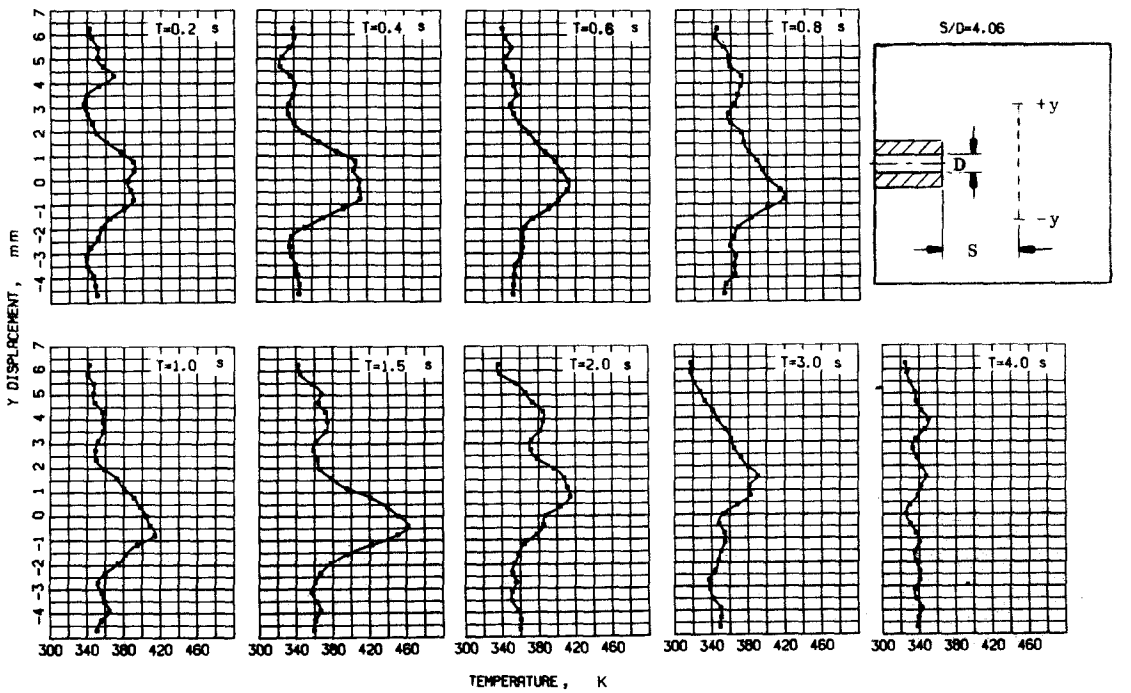

FIG. 8. Temperature profiles at 4.06 tube diameters from inlet.

reached (at about 2.0 s) and the temperature slowly decreases back to room temperature.

The density profiles show a strong correlation with the corresponding temperature profiles for all times and distances from the jet inlet. The density profiles are plotted in an inverse manner to make this correlation more clear. The density profiles for the test configuration of $S/D = 4.06$ are shown in Fig. 10.

Inferred flow field

Even though extensive data were taken, the complete specification of the flow field is so complex as to require an overwhelming amount of additional data from regions beyond those where data were obtained. Thus, great care must be taken in deducing the probable flow field from temperature profiles. However, the following general trends can be inferred from the

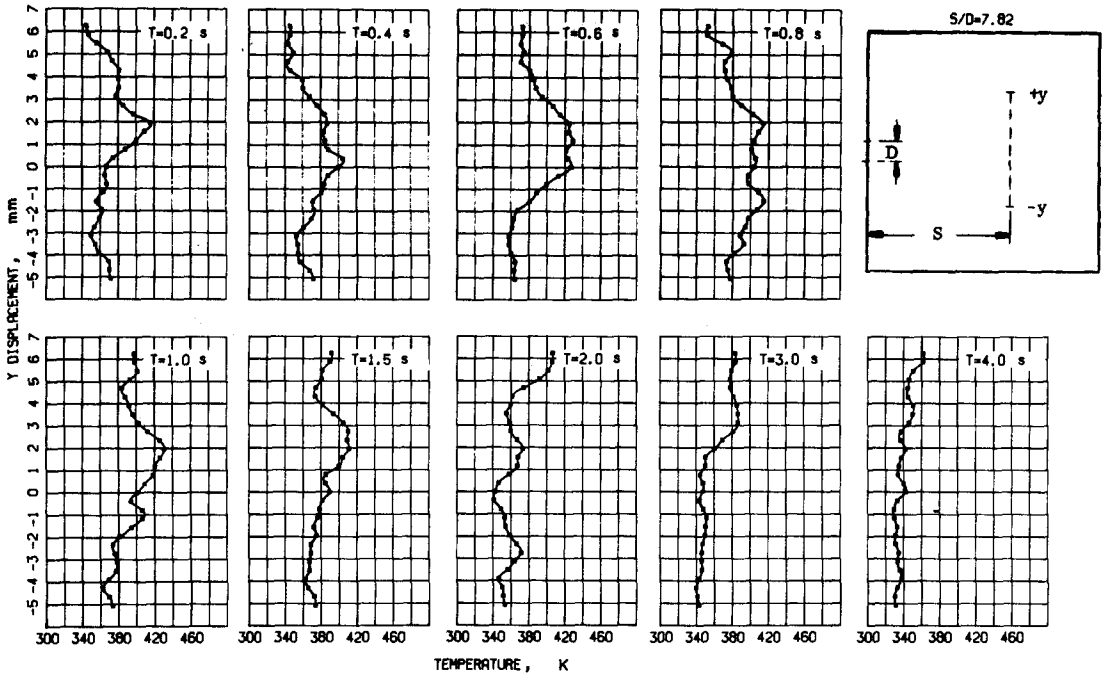

FIG. 9. Temperature profiles at 7.82 tube diameters from inlet.

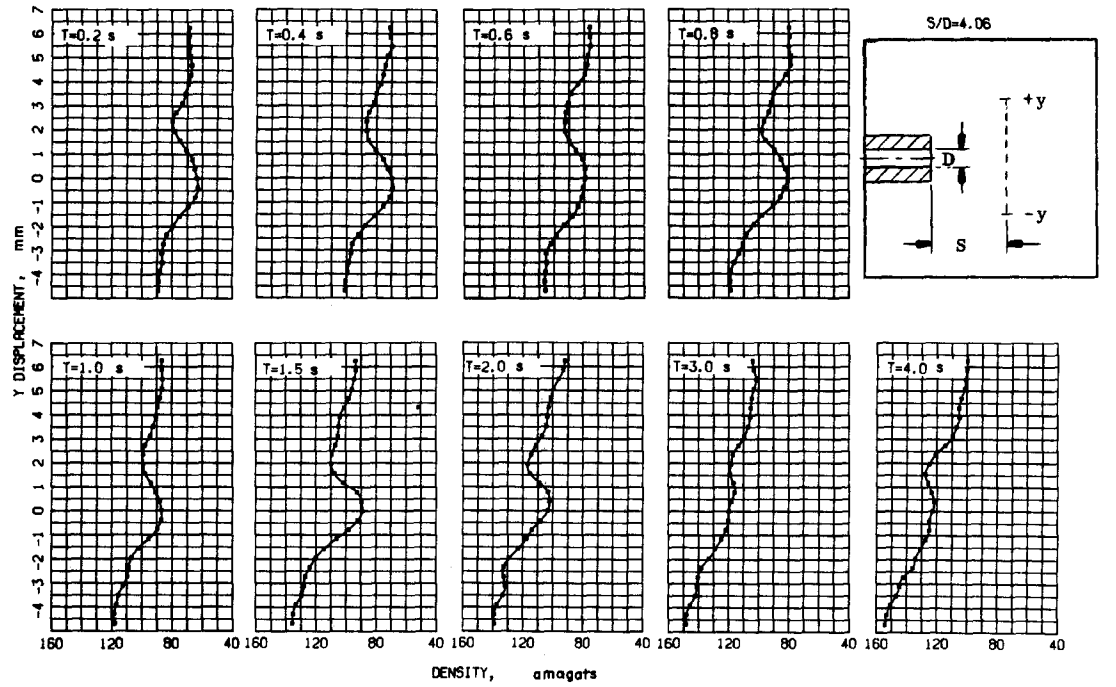

FIG. 10. Density profiles at 4.06 tube diameters from inlet.

measured profiles. All axial injection configurations show a well-defined jet region near the axis of the test cell during the first 2 s of the filling process. The center of the jet is marked by the highest temperature and lowest density, while the jet boundaries are marked by the return of the temperature to values near those found at the extremes of the spatial range (i.e. temperature values at the y displacement extremes).

A warm region is almost always found above the jet, and sometimes there is a smaller warm region below the jet. This pattern is thought to be caused by recirculating flow in the following manner. As the warm jet flows along the cylinder axis, a portion of it hits the end wall, flows back around the sides of the cylinder (where it is cooled significantly by heat transfer to the room-temperature walls), and then turns toward the

inlet region. There, entrainment of some of this cooled gas results in coflow with the jet, an occurrence indicated by the presence of a cool region above and below the incoming warm jet. The concurrent presence of a warmer region – also above and below, but farther from the jet – occurs because the lower-velocity peripheral portion of the warm jet does not impinge on the cell walls and this is cooled much less. This gas is thought to be rolled into a toroidal vortex between the end wall and the inlet. As an example of the flow-field changes with time, the flow inferred from the temperature profiles obtained at 4.06 diameters from the inlet are shown in Fig. 11.

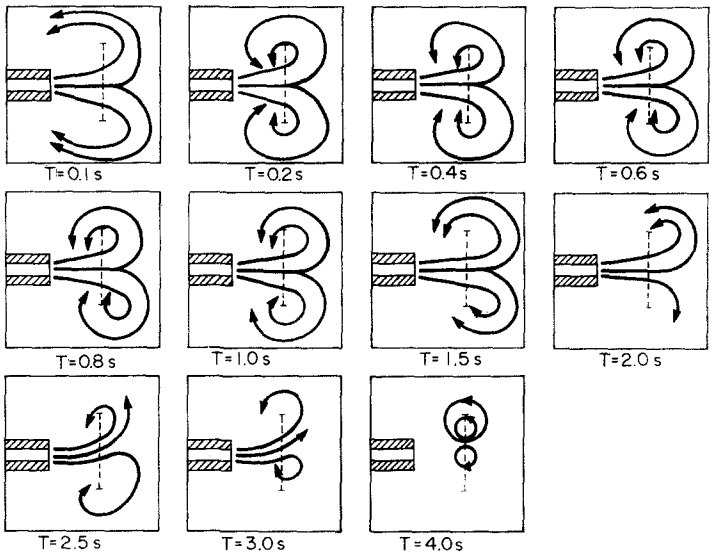

FIG. 11. Inferred flows from profiles at 4.06 diameters from inlet.

Comparison of the early-time temperature profiles of Fig. 7 ($S/D = 0.94$) and Fig. 9 ($S/D = 7.82$) indicates a slight upward curvature of the jet from the test-cell axis of symmetry. The late-time temperature profiles for all configurations suggest significant upward flow as the inlet jet velocity approaches zero. This effect is due to buoyant force on the lower density jet.

Since the inlet valve was not closed until long after pressure equilibrium was achieved, cooling of the test-cell gas at late times by heat transfer to the cell walls causes a very slow laminar jet to continue to be injected. The typical angle between these thermally induced laminar jets and the test-cell centerline is of the order of 18–25 degrees. Again, this deflection is thought to be caused by buoyancy of the warm jet.

Comparison of data with free-jet characteristics

In the region near the test cell centerline at early times, the flow field is dominated by the jet. The boundaries of the core of the jet are clearly visible in the early temperature profiles at 0.94 diameters from the inlet (Fig. 7). The core diameter in this region is about 1.2 mm, or 0.6 of the inlet diameter. Corrsin and Uberoi's [22] data on a similar hot, turbulent, free (unconfined) jet indicate a core length of about three diameters, with a core diameter of 0.68 inlet diameter at the same location.

The point where the temperature is one-half the temperature difference between the centerline and edge temperatures makes an angle with the jet centerline of about 9 degrees. Tollmein's analysis [23] of the axially symmetric free jet predicts a thermal spreading angle of 7–8 degrees.

The late-time temperature profiles show a probable transition to laminar flow in the jet at 1.5–2 s. This occurrence is indicated by the narrow, high-temperature jet at 1.5 s in Fig. 8. At still later times, the temperature profiles are dominated by the residual toroidal flow field, which gives rise to the characteristic double-peak profile. Late-time profiles usually show a considerable temperature variation, with warm gas at the top of the test cell. Regions at the cross-sectional centers of the toroid tend to keep the jet centerline temperature from decreasing as fast as that of a free jet.

SUMMARY AND CONCLUSIONS

A system utilizing rotational Raman scattering has been developed to simultaneously measure static temperature and concentration profiles in diatomic gases during transient flow. The nonrigid-rotator molecular model of deuterium used is in good agreement with the rotational Raman spectra taken. The system recorded spectra every 0.033 s with time resolution of 0.1 s, and a spatial resolution of 0.2 mm. Temperature accuracy was of the order of ± 10 K, and concentration accuracy was of the order of $\pm 10\%$.

The rotational Raman profile system has been applied to the measurement of temperature and concentration profiles during the transient filling of a right circular cylinder by axial injection of warm (430 K) deuterium at 200 atm into room temperature (300 K) deuterium at 100 atm. On the basis of the measured temperature profiles, the transient filling process for

the geometry used appears to result in a varying flow field that exhibits a jet region near the inlet and a toroidal flow field midway between the inlet and the end wall. Although the jet region behaves like a free jet, free-jet theory does not describe the main region of the jet because of the presence of recirculating flow.

The jet makes a transition from turbulent to laminar flow about 1.5 s after the start of the filling process. Also noted at late times was the growing influence of buoyant forces causing the warmer gas to drift upward in the cylinder; and even though the pressure equalizes between the source vessel and the test cylinder at about 2 s, a toroidal flow field persists for as long as 4–5 s. At all times, the temperature and concentration profiles show a strong correlation which is consistent with the nearly uniform pressure field within the test cylinder.

REFERENCES

1. S. Lederman and J. Bornstein, Application of Raman effect to flowfield diagnostics, in *Instr. for Airbreathing Prob., Progress in Astronautics and Aeronautics Series*, edited by A. E. Fuhs and M. Kingery, Vol. 34, p. 283. MIT Press, Cambridge, Massachusetts (1974).
2. A. C. Eckbreth, Laser Raman thermometry experiments in simulated combustor environments, AIAA Paper No. 76-27 (1976).
3. C.-S. Wange, Theory of stimulated Raman scattering, *Phys. Rev.* **182**(2), 482–494 (June 1969).
4. H. J. Neusser and H. Puell, Density distribution in a high-pressure gas jet measured by laser-induced gas breakdown, *Physics Fluids* **15**(7), 1355–1358 (July 1972).
5. J. J. Barrett and N. I. Adams, III, Laser-excited rotational–vibrational Raman scattering in ultra-small gas samples, *J. Opt. Soc. Am.* **58**(3), 311–319 (March 1968).
6. M. Bridoux, A. Chapput, M. Crunelle and M. Delhaye, New trends in rapid laser-Raman spectroscopy, in *Advances in Raman Spectroscopy*, edited by J. P. Mathieu, Vol. 1, pp. 65–69. Heyden, London (1973).
7. G. F. Widhopf and S. Lederman, Specie concentration measurements utilizing the Raman scattering of a laser beam, Polytechnic Institute of Brooklyn, Rpt. No. 69-46 (1969).
8. J. A. Salzman, W. J. Masica and T. A. Coney, Determination of gas temperatures from laser-Raman scattering, NASA TND-6336, Lewis Research Center, Cleveland, Ohio (1971).
9. P. Fong, *Elementary Quantum Mechanics*, pp. 150–157. Addision-Wesley, Reading, MA (1962).
10. G. Herzburg, *Molecular Spectra and Molecular Structures*, Vol. 1, *Spectra of Diatomic Molecules*, p. 128. Van Nostrand–Reinhold, New York (1950).
11. W. G. Vincenti and C. H. Kruger, Jr., *Introduction to Physical Gas Dynamics*, pp. 132–133. John Wiley, New York (1965).
12. G. Placzek and E. Teller, Die Rotationsstruktur der Ramanbanden mehratomiger Moleküle, *Phys. Z.* **81**, 209–258 (1933).
13. T. C. James and W. Klemperer, Line intensities in the Raman effect of $^1\Sigma$ diatomic molecules, *J. Chem. Phys.* **3**(1), 130–134 (1959).
14. J. R. Smith, A rotational Raman scattering system for measuring temperature and concentration profiles in transient gas flows, Ph.D. Dissertation, U. C. Davis (February 1975).
15. J. A. Cooney, Measurement of atmospheric temperature profiles by Raman backscatter, *J. Appl. Meteorol.* **11**, 108 (1972).
16. A. A. Boiarski, Shock-tube diagnostics utilizing laser Raman spectroscopy, Naval Surface Weapons Center, Tech. Report WOL/TR-75-53 (April 1975).
17. T. A. Coney and J. A. Salzman, Determination of the temperature of gas mixtures by using laser Raman scattering, NASA Tech. Note D-7126 (January 1973).
18. J. R. Murray and A. Javan, Effects of collisions on Raman line profiles of hydrogen and deuterium, *J. Molec. Spectros.* **42**, 1–26 (1972).
19. G. E. Devlin, J. L. Davis, L. Chase and S. Geschwind, Absorption of unshifted scattered light by a molecular I_2 filter in Brillouin and Raman scattering, *Appl. Phys. Letters* **19**(5), 138–141 (September 1971).
20. M. Lapp, C. M. Penney and J. A. Asher, Application of light-scattering techniques for measurements of density, temperature and velocity in gas dynamics, Aerospace Research Laboratories, U.S. Air Force Systems Command, Wright-Patterson AFB, Ohio, ARL-73-0045, p. 12 (April 1973).
21. E. J. Stansbury, M. F. Crawford and H. L. Welsh, Determination of rates of change of polarizability from Raman and Rayleigh intensities, *Can. J. Phys.* **31**, 954–961 (1953).
22. S. Corrsin and M. S. Uberoi, Further experiments on the flow and heat transfer in a heated turbulent air jet, NACA Report No. 998 (1950).
23. G. N. Abramovich, *The Theory of Turbulent Jets*, p. 81. M.I.T. Press, Cambridge, MA (1963).

PROFILS DE TEMPERATURE ET DE CONCENTRATION DANS LES ECOULEMENTS GAZEUX INSTATIONNAIRES PAR LA DIFFUSION RAMAN ROTATIONNELLE

Résumé—On présente une technique nouvelle pour mesurer simultanément les profils de température et de concentration dans les gaz diatomiques en écoulement instationnaire. Utilisant un laser continu à argon, la lumière diffusée par effet Raman à travers les gaz échantillons est dispersée par un spectromètre à un seul passage; les spectres résultant sont détectés par un intensificateur d'image et une caméra de télévision à faible niveau de lumière, à intervalle de 0,033 s.

Un système basé sur cette technique a été réalisé et des distributions de température et de concentration ont été obtenues pour un cylindre circulaire droit et une injection de deutérium à 200 atm et 430 K dans du deutérium à 100 atm et 300 K. Des profils de température et de concentration sont présentés à des époques différentes pendant l'injection.

BESTIMMUNG VON TEMPERATUR- UND KONZENTRATIONSPROFILEN IN INSTATIONÄREN GASSTRÖMUNGEN MIT HILFE DER ROTATIONS-RAMAN-STREUUNG

Zusammenfassung—Es wird eine neue Technik zur gleichzeitigen Messung von Temperatur- und Konzentrationsprofilen in 2-atomigen Gasen bei instationärer Strömung vorgestellt. Unter Verwendung eines kontinuierlichen Argonlasers wird Rotations-Raman-Streulicht aus den Probegasen in einem

Einweg-Spektrometer gestreut; die resultierenden Spektren werden in Zeitabständen von 0,033 s über einen Bildverstärker und eine schwachlichtauflösende Fernsehkamera aufgenommen. Ein auf dieser Methode basierendes System wurde entwickelt und damit die Temperatur- und Konzentrationsverteilungen in einem Kreiszylinder bei axialer Einspritzung von Deuterium bei 200 atm und 430 K in Deuterium von 100 atm und 300 K bestimmt. Für ausgewählte Zeitpunkte während des Einspritzvorganges werden Temperatur- und Konzentrationsprofile angegeben.

ПРОФИЛИ ТЕМПЕРАТУРЫ И КОНЦЕНТРАЦИИ В НЕУСТАНОВИВШИХСЯ ПОТОКАХ ГАЗА, ПОЛУЧЕННЫЕ МЕТОДОМ ВРАЩАТЕЛЬНОЙ СОСТАВЛЯЮЩЕЙ РАМАНОВСКОГО РАССЕЯНИЯ

Аннотация — Рассматривается новый метод одновременного измерения профилей температуры и концентрации в неустановившихся потоках двухатомных газов. Полученная с помощью аргонового лазера непрерывного действия вращательная составляющая Рамановского рассеяния образцов газов анализируется одноканальным спектрометром, причем спектры детектируются каждые 0,033 сек. с помощью электронного видеоусилителя и телевизионной установки высокой разрешающей способности.

На основе этого метода была создана система и определены профили температуры и концентрации в круглом цилиндре правильной формы во время инжекции дейтерия в аксиальном направлении при 200 ат и 430 К в дейтерий при 100 ат и 300 К. Профили температуры и концентрации представлены для определенных моментов времени в процессе инжекции.